● RESEARCH ARTICLE

Sciatic nerve injury alters the spatial arrangement of neurons and glial cells in the anterior horn of the spinal cord

Ali Rashidiani-Rashidabadi[1, #], Mohammad Hassan Heidari[1], Ensieh Sajadi[1], Fatemeh Hejazi[2], Fatemeh Fadaei Fathabady[1], Yousef Sadeghi[1], Abbas Aliaghaei[1], Amir Raoofi[1], Mohammad-Amin Abdollahifar[1, *, #], Reza Mastery Farahni[1, *]
1 Department of Biology and Anatomical Sciences, School of Medicine, Shahid Beheshti University of Medical Sciences, Tehran, Iran
2 Department of Polymer Engineering and Color Technology, Amirkabir University of Technology (Tehran Polytechnic), Tehran, Iran

Funding: *The work was supported by the Research Vice-chancellor of Shahid Beheshti University of Medical Sciences, Tehran, Iran (No. 1394-373; to RMF).*

Abstract
The spatial arrangement of the cell is important and considered as underlying mechanism for mathematical modeling of cell to cell interaction. The ability of cells to take on the characteristics of other cells in an organism, it is important to understand the dynamical behavior of the cells. This method implements experimental parameters of the cell-cell interaction into the mathematical simulation of cell arrangement. The purpose of this research was to explore the three-dimensional spatial distribution of anterior horn cells in the rat spinal cord to examine differences after sciatic nerve injury. Sixteen Sprague-Dawley male rats were assigned to control and axotomy groups. Twelve weeks after surgery, the anterior horn was removed for first- and second-order stereological studies. Second-order stereological techniques were applied to estimate the pair correlation and cross-correlation functions using a dipole probe superimposed onto the spinal cord sections. The findings revealed 7% and 36% reductions in the mean volume and total number of motoneurons, respectively, and a 25% increase in the neuroglial cell number in the axotomized rats compared to the control rats. In contrast, the anterior horn volume remained unchanged. The results also indicated a broader gap in the pair correlation curve for the motoneurons and neuroglial cells in the axotomized rats compared to the control rats. This finding shows a negative correlation for the distribution of motoneurons and neuroglial cells in the axotomized rats. The cross-correlation curve shows a negative correlation between the motoneurons and neuroglial cells in the axotomized rats. These findings suggest that cellular structural and functional changes after sciatic nerve injury lead to the alterations in the spatial arrangement of motoneurons and neuroglial cells, finally affecting the normal function of the central nervous system. The experimental protocol was reviewed and approved by the Animal Ethics Committee of Shahid Beheshti University of Medical Sciences (approval No. IR.SBMU.MSP.REC1395.375) on October 17, 2016.

Key Words: *sciatic nerve injury; spatial arrangement; spinal cord; motorneuron; neuroglial cells; axotomy; anterior horn*

Chinese Library Classification No. *R446; R361; Q2*

Correspondence to:
Reza Mastery Farahani, PhD, realmastery@hotmail.com or dr.farahani@sbmu.ac.ir;
Mohammad-Amin Abdollahifar, PhD, m_amin58@yahoo.com or abdollahima@sbmu.ac.ir.

#These authors contributed equally to this work.

orcid:
0000-0002-3037-4236 (Reza Mastery Farahani)
0000-0001-6947-3285 (Mohammad-Amin Abdollahifar)

doi: *10.4103/1673-5374.257539*

Received: *November 24, 2018*
Accepted: *March 19, 2019*

Introduction
Injury to the sciatic nerve is relatively common and can be caused by crushing, wounds, fractures or surgical intervention (Sun et al., 2009a; Yin et al., 2010). The sciatic nerve is a mixed nerve that contains motor, sensory and autonomic fibers (Li et al., 2006); thus, injury to this nerve usually leads to significant motor, sensory, and autonomic dysfunctions (Sun et al., 2009b). Despite the numerous techniques for the treatment of nerve injury, nerve regeneration is hindered by the following factors: Wallerian degeneration of axons distal to the site of the lesion (Brodal, 1981) and neuronal apoptosis at the corresponding spinal segments (Chen et al., 2013; Lu et al., 2014; Preyat et al., 2015).

Neuronal apoptosis can be induced by lack of neurotrophic factors when retrograde axonal transport is interrupted following axonal injury, preventing neurotrophic factors from being delivered to neuronal bodies from the target organs (Tong and Rich, 1997; Nakamura and Myers, 2000). In addition, simultaneous Ca^{2+} influx results in disturbance in intracellular Ca^{2+} homeostasis and subsequent activation of proteolytic enzymes. This initiates a number of immune responses that lead to neuronal apoptosis (Preyat et al., 2015). Motoneuron apoptosis is characterized by chromatolysis followed by progressive condensation in the cytoplasm and nucleus (Martin, 1999) and accumulation of neurofilaments in the proximal axon and perikaryon (Manetto et al., 1988; Munoz et al., 1988). These events lead to motoneuron loss in the anterior horn and will undoubtedly alter the spatial distribution of motoneurons, neuroglia and the relationship between them.

Aside from reports on the quantitative aspects of the anterior horn (Mayhew et al., 1979; Bjugn et al., 1993; Low et al., 2003; Kakinohana et al., 2004; Walloe et al., 2011), no research has addressed the spatial distribution of cells in the anterior horn. Little is reported about the effects of spatial arrangement of neurons and glial cells in the spinal cord after sciatic nerve injury. Therefore, the aim of this study was to investigate the relationship between the spatial arrangement alteration of neurons and glial cells in the anterior horn of spinal cord after axotomy with the first order and second order stereological methods.

Materials and Methods

Animals

Sixteen Sprague-Dawley male rats, weighing 220–260 g, were purchased from Laboratory Animal Center of Pasteur Institute, Tehran, Iran. The experimental protocol was reviewed and approved by the Animal Ethics Committee of Shahid Beheshti University of Medical Sciences (approval No. IR.SBMU.MSP.REC1395.375) on October 17, 2016. The rats were randomly allocated to the control (normal control) and axotomy groups (n = 8/group) and were maintained under standard laboratory conditions. Anesthesia induction was achieved in the axotomy group with ketamine hydrochloride (50 mg/kg) plus xylazine hydrochloride (20 mg/kg). After disinfection, the skin and underlying muscles of the right hind limb were incised along the femoral axis and a 1-cm-long segment of the sciatic nerve was transected.

Tissue preparation

At 12 weeks after surgery, the animals were sacrificed by deep anesthesia and then perfused intracardially using 0.9% physiological saline and 4% paraformaldehyde. After extraction of the spinal cord, samples were obtained from the corresponding spinal segments (L4 and L5) (Gelderd and Chopin, 1977) and were maintained in 4% paraformaldehyde for 7 days. Complete paraffin serial sections (10 and 25 μm thick) were made using a microtome (Leica RM2125; Nnussloch, Germany). By systematic uniform random sampling, 10 sections of each sample were selected by randomly choosing a numbered sample (between 1 and 10). The sample then was stained with hematoxylin & eosin (H&E; Sigma, St. Louis, MO, USA) and Cresyl violet (Sigma). The sections were evaluated in stereological software (Stereo Investigator, Williston, VT, USA), and the anterior horn volume, motoneuron mean volume, and motoneuron and neuroglial cell numbers were estimated (Gundersen et al., 1988a, b).

Total volume of the anterior horn of the spinal cord

Cavalieri's principle was applied for the assessment of the anterior horn volume using the following equation (Gundersen et al., 1988a, b; Noorafshan et al., 2014):

$$V_{total} = \sum P \times \frac{a}{p} \times t$$

where ΣP is the sum of the falling points on the anterior horn histological sections, a/p is the area per point and t is the distance among the sections (**Figure 1**).

Motoneuron mean volume

The nucleator method was applied to estimate the motoneuron mean volume as:

$$V_n = \frac{4\pi}{3} \times l_n$$

where l_n are two horizontal directions from the central point of the nucleolus to the cell borders (Gundersen et al., 1988a, b; Noorafshan et al., 2014) (**Figure 2**).

Motoneuron and neuroglial cell numbers

The optical dissector method was applied to estimate the motoneuron and neuroglial cell number in the anterior horn (Gundersen et al., 1988b; Noorafshan et al., 2014). The anterior horn cell nucleus distribution was assessed in the z-axis. There are ten columns and each column represents the percent of the counted nuclei in 10% of the tissue section thickness (**Figure 3A**). The numerical density (N_v) of the motoneurons and neuroglial cells was calculated as:

$$N_v = \frac{\sum Q}{\sum P \times h \times \frac{a}{f}} \times \frac{t}{BA}$$

where (ΣQ) is the sum of the cells with nuclei, ΣP is the sum of counting frame, h is the dissector height, a/f is the area of the frame, t is the real thickness of the section and BA is the microtome section thickness (**Figure 3B** and **C**). The total number of motoneurons and neuroglial cells was calculated as:

$$N_{total} = N_v \times V$$

In this formula, N_v is the numerical density of neurons and glial cells and V is the total volume of anterior horns.

Glial fibrillary acidic protein expression

Immunohistochemical staining was used to analyze the expression of glial fibrillary acidic protein (GFAP), an astrocyte marker, in the sections of the anterior horn. First, the tissue section slides were deparaffinized in xylene (Merck, Darmstadt, Germany) and the slides were immersed in ethanol (Merck) for rehydration. Afterwards, the tissue slides were transferred to a 10 mM sodium citrate buffer (Sigma) at pH 6.0 for antigen retrieval. The endogenous peroxidase was blocked by tissue incubation in 3% hydrogen peroxide. Among incubations, two washes were performed with Tris/HCl buffer (Sigma) at pH 6.0. Next, tissue samples were incubated with rabbit polyclonal anti-GFAP antibody (1:250; Invitrogen, Carlsbad, CA, USA) with immunoglobulin overnight at 4°C and then with biotinylated goat anti-mouse antibody (1:200; Invitrogen) for 2 hours at room temperature according to manufacturer instructions. Visualization of immunoreactivity was achieved after incubation of the tissue sections in diaminobenzidine solution (0.1%; Sigma). Finally, counterstaining was performed using Harris-modified hematoxylin solution (Sigma).

TUNEL assay

Apoptosis was evaluated by TUNEL staining to analyze DNA damage. After axotomy, the spinal cord tissues were fixed and embedded in paraffin and then sectioned on glass slides. Staining was performed according to TUNEL protocol (In Situ Apoptosis Detection Kit, Roche, Mannheim, Germany). Finally, the percentage of TUNEL-positive cells was calculat-

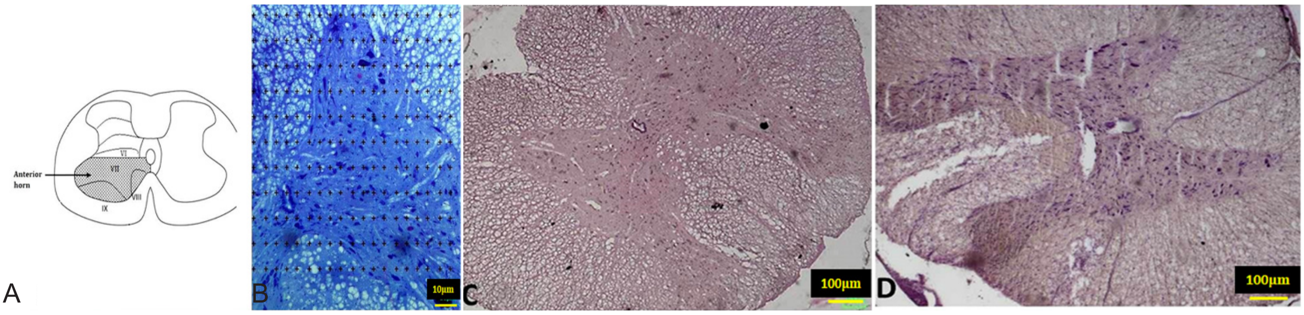

Figure 1 Total volume of the anterior horn of the spinal cord.
(A) Schematic of transverse section of L5 spinal cord of animals from the control and axotomy groups. The anterior horn of the spinal cord consists of Rexed laminae VII–VIII and IX. Lamina VII forms the central part of the anterior horn. Lamina VIII occupies the antero-medial part of the anterior horn. Lamina IX is located in the most anterior and lateral parts of the anterior horn; (B) photomicrograph of the spinal cord stained with Cresyl violet (original magnification, 4×). Scale bar: 10 μm. A point grid is superimposed over the photomicrograph for measuring the anterior horn volume (AH denotes anterior horn); (C, D) photomicrographs of the spinal cord stained with hematoxylin & eosin (original magnification, 4×) from the control and axotomy groups, respectively. Scale bar: 100 μm.

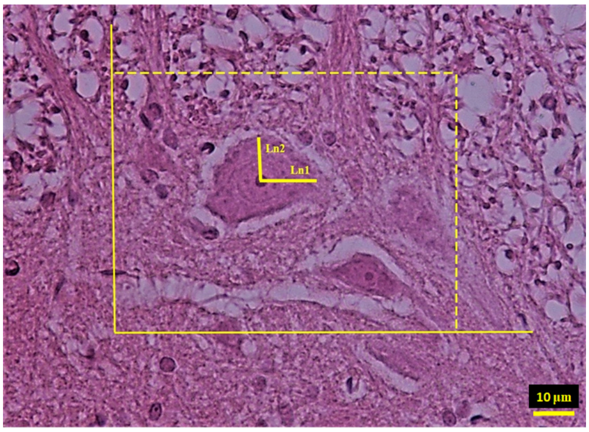

Figure 2 Motoneuron mean volume in the anterior horn of the spinal cord.
Photomicrograph of the anterior horn stained with hematoxylin and eosin (original magnification, 40×). Scale bar: 10 μm. Ln is the distance in two directions from the center of the nucleolus to the motoneuron borders for estimating the mean volume of the anterior horn motoneuron. Counting frames are superimposed over the photomicrographs to measure motoneuron mean volume. The yellow box is counting frame.

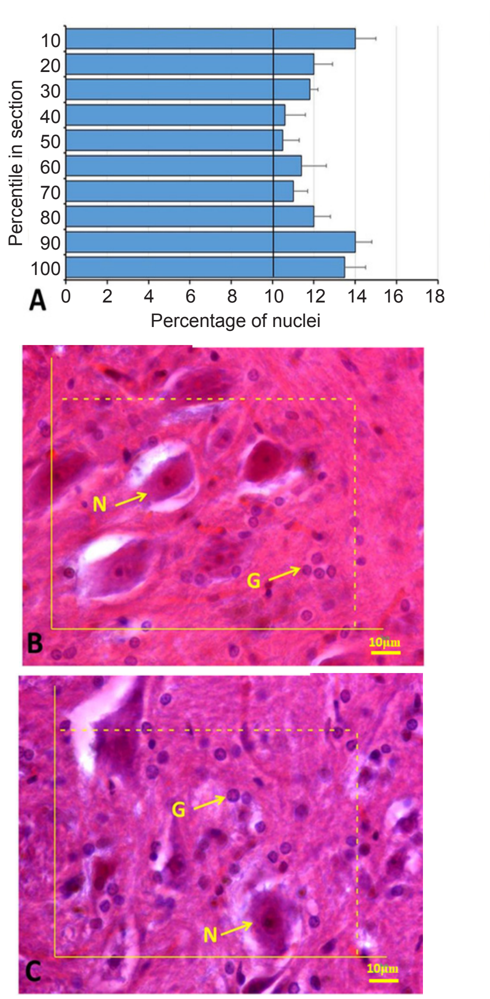

Figure 3 Motoneuron and glial cell numbers in the anterior horn of the spinal cord.
(A) Anterior horn cell nucleus distribution on z-axis. Each of the 10 histograms shows the percentage of located cell nuclei in 10% of the tissue section; (B, C) photomicrographs of the anterior horn stained with hematoxylin & eosin (original magnification, 40×). Counting frames are superimposed over the photomicrographs to measure the number of motoneurons (N) and neuroglial cells (G). The yellow box is counting frame. Scale bars: 10 μm.

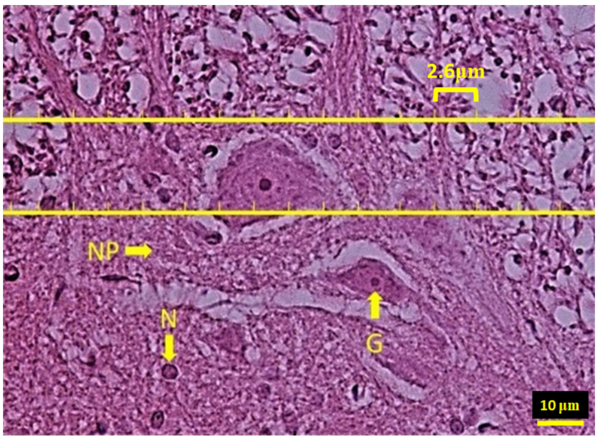

Figure 4 The micrograph illustrating the codes of cells in the spinal cord for creating a data matrix.
The distance (r = 2.6 μm) between two points of grid is 2.6 μm. Each point of the grid is coded in Figure 9 as 1, 2 and 3 if the point is placed over the motoneuron (N), neuroglial cell (G), and neuropil (NP), respectively. Scale bar: 10 μm.

ed in three sections per sample by stereological methods.

Coefficient of error (CE)

CE (*V*) was calculated using the following equation:

$$CE(V) = (\Sigma P^{-1}) \times [\frac{1}{12}(3\Sigma P_i^2 + \Sigma P_i P_{i+2} - 4\Sigma P_i P_{i+1})^{1/2}$$

where *CE(V)* is the *CE* for determining the total volume of the anterior horn of the spinal cord. In this formula, *P* and P_i are the sum of the falling points on the anterior horn histological sections. The *CE* for determining the number of motoneurons and neuroglial cells and the total volume of the anterior horn of the spinal cord was calculated as follows (Gundersen and Jensen, 1987):

$$CE(N) = [CE^2(N_v) + CE^2(V)]^{1/2}$$

$$CE(N_v) = [\left(\frac{n}{n-1}\right) \times \left[\left(\frac{\Sigma(Q)^2}{(\Sigma Q)^2}\right) + \left(\frac{\Sigma(P)^2}{(\Sigma P)^2}\right) - \left(\frac{2\Sigma(QP)}{\Sigma Q \Sigma P}\right)\right]]^{1/2}$$

Table 1 shows the values of the CEs.

Covariance function

The covariance of a component (*X*) was estimated as follows (Mayhew, 1999a, b; Reed and Howard, 1999; Reed et al., 2010):

$$C(r)X = \frac{\sum \boldsymbol{DP(X,r)}}{\sum \boldsymbol{DP(ref,r)}}$$

Both end points of the dipoles (DP) of class size $r = 1$ (equivalent to 2.6 μm) had a chance of being included in the same cell profile. When evaluating *Vv*, *C*(*r*), and *g*(*r*), the distance among the points (*DP*) ranged from $r = 0$ (equivalent to 0 μm) to $r = 49$, making the total distance of 127.4 μm (49 × 2.6 = 127.4 μm) (**Figure 4**). MATLAB software (version R2016a; Math Works, Plano, TX, USA) was used to convert the data matrix to image type.

Pair correlation function

The pair correlation function is the normalized covariance function obtained by dividing the covariance by the reference value (squared volume fraction) as follows (Mayhew, 1999a, b; Reed and Howard, 1999; Reed et al., 2010):

$$g(r) = \frac{C(r)}{Vv^2}$$

In this formula, *C*(*r*) is covariance and Vv^2 is the reference value (squared volume fraction).

Cross-covariance function

The cross-covariance (*C*(*r*)*X*, *Y*) was applied to spatial arrangement quantification and evaluated as follows (Mattfeldt et al., 1993, 2006; Mayhew, 1999a, b; Reed and Howard, 1999; Krasnoperov and Stoyan, 2004; Reed et al., 2010):

$$C(r)X = \frac{\sum \boldsymbol{DP(X,r)}}{\sum \boldsymbol{DP(ref,r)}}$$

In this formula, *DP* (*XY*, *r*) and *DP* (*ref*, *r*) are the dipole length which hit the favored structure (neuron or glia) and the nervous tissue, respectively.

Cross-correlation function

The cross-correlation is normalized to remove volume fraction differences by the evaluation of cross-correlation function as follows (Reed and Howard, 1999; Reed et al., 2010; Mayhew, 1999a, b):

$$g(r)XY = \frac{C(r)XY}{Vv(X,\mathrm{ref}) \times Vv(Y,\mathrm{ref})}$$

In this formula, *C*(*r*)*XY* is the cross-covariance between the two components (*X*, *Y*) is defined as the probability that an isotropic dipole of length "*r*" hits components *X* and *Y* simultaneously divided by the number of the dipoles hitting the reference volume (*Vv*) *X* and *Y* ref.

Statistical analysis

All data analyses were accomplished by the Mann-Whitney *U* test, Pfaffl method and one-way analysis of variance with $P \le 0.05$ being considered significant. Coefficients of variation among animals (CV = mean ± SD) were calculated for neuron and glia volume within spinal cord. *g*(*r*) of the neurons and glial cells and cross-correlation were compared between groups using Mann-Whitney *U* test.

Results

Motoneuron and neuroglial cell numbers in the anterior horn of the spinal cord

Assessment of the anterior horn sections of the spinal cord revealed significantly lower numbers of motoneurons (~36%) in the axotomized animals compared to the control animals (**Figure 5A**). Significantly more neuroglial cells (~25%) were observed in the axotomized animals compared to the control animals (**Figure 5B**).

Mean volume of motoneurons and total volume of the anterior horn of the spinal cord

The results showed that the mean volume of the motoneurons was significantly lower by ~7% in the axotomized ani-

Table 1 Coefficients of error (CE) for total volume of the anterior horn and the number of neurons and glial cells

Group	Volume of the anterior horn	Numerical density of neurons	Numerical density of glial cells	Number of neurons	Number of glial cells
Control (*n* = 6)	0.04	0.05	0.05	0.05	0.03
Axotomy (*n* = 6)	0.03	0.04	0.03	0.04	0.04

mals compared to the control animals (**Figure 5C**). However, the total volume of the anterior horn remained unchanged (**Figure 5D**).

GFAP expression

GFAP expression in the anterior horn was significantly up-regulated in the axotomized animals compared to the control animals (**Figure 6**).

TUNEL assay

The effect of axotomy on apoptotic changes in the anterior horn motoneurons was investigated by TUNEL assay. $TUNEL^+$ cell counts showed that apoptosis was significantly enhanced in the axotomized animals compared to the control animals (**Figure 7**).

Conversion of data matrix to image type

Sciatic nerve axotomy altered the spatial distribution of the motoneurons and neuroglial cells such that these cells were dissociated in most places. To better understand what occurred, the data matrices of the control and axotomy groups were converted to image types in MATLAB (**Figure 8**).

Spatial arrangement of motoneurons

The $g(r)$ for motoneurons *versus* the dipole distance, r, was plotted (**Figure 9A**). The estimated values from the beginning to the end of the curve (r = 0 to 7.8 μm, r = 18.2 to 54.6 μm, r = 59.8 to 75.4 μm, r = 80.6 to 91 μm, and r = 109.2 to 119.6 μm) revealed a significant difference between groups. After the gap, the data points for both groups were arranged randomly at longer distances ($P < 0.05$).

Spatial arrangement of neuroglial cells

The $g(r)$ for neuroglia *versus* dipole distance, r, was plotted (**Figure 9B**). The estimated values from the beginning to the end of the curve (r = 0 to 5.2 μm, r = 46.8 to 57.2 μm, r = 80.6 to 88.4 μm and r = 114 to 124.8 μm) revealed a significant difference between groups. After the gap, the data points for both groups were arranged randomly at longer distances ($P < 0.05$).

Cross-correlation of motoneurons and neuroglial cells

The cross-correlation curve shows a negative correlation between the motoneurons and neuroglial cells at 20.8–36.4, 85.8–88.4 and 117–127.4 μm of the axotomized animals compared to the control animals ($P < 0.05$). When the cross covariance was located above the reference line, a positive correlation among components was indicated. When the cross covariance was located below the line, a negative correlation was indicated. The findings in the present work indicate that there was a positive correlation among the anterior horn cells in the control animals, but a negative correlation in the axotomized animals (**Figure 9C**).

Discussion

The spatial distribution of the cells was strongly associated with their interactions. One hypothesis states that spatial cell distribution is related to cellular behavior of coordinates. In a multicellular organ, cells function through spatial distribution in the tissues (Altomare and Fare', 2008; Ekerdt et al., 2013). The cell-to-cell interaction relates to normal functioning of the organ; however, changes in these cell-to-cell interactions can result in abnormal tissue physiology related to disease (Altomare and Fare', 2008; Ekerdt et al., 2013).

In this study, we obtained an accurate evaluation and unique quantitative analysis of the cellular spatial patterns in the anterior horn. The present work determined the quantitative alterations in spatial distribution of the motoneurons and neuroglial cells within the anterior horn using second-order stereology. Our findings demonstrate that total number and mean volume of the motoneurons decreased in the anterior horn after sciatic nerve injury. We also found significantly more neuroglial cells in the axotomized animals compared to the control animals. The positive astrocytic GFAP in the anterior horn was also significantly different between groups. These can be linked to the altered spatial distribution in the anterior horn. The pair-correlation curve for motoneurons and neuroglial cells indicated a broader gap in their spatial distribution in the axotomy group. Of course, these gaps could be filled with neurophil. The cross-correlation function also showed that the motoneurons and neuroglial cells in the axotomy group were negatively correlated.

The mechanisms underlying motoneuron/motoneuron, neuroglial/neuroglial and motoneuron/neuroglial communication after axotomy remain poorly understood. Several mechanisms could be responsible for the disturbance in the spatial distribution of the anterior horn cells after axotomy. Peripheral nerve axotomy results in motoneuron apoptosis by expression of the genes involved in promoting apoptosis, including the apoptotic activator factor 1, Bax, caspase-3 and caspase-9 and triggers intracellular death pathways. Moreover, sciatic nerve injury causes necrosis of the gray matter, followed by destruction of the motoneurons, neuroglial cells and blood vessels, increasing the glutamate concentration and decreasing the cAMP (Sendtner et al., 1992; Griffin et al., 1995; Oppenheim et al., 1995).

The findings obtained in this work were consistent with those of our previous study that showed alterations in the neuronal and neuroglial distribution of the rat prefrontal cortex following chronic stress (Noorafshan et al., 2015). In another study, we reported that the spatial pattern of cerebellar Purkinje cells altered following 3-acetylpyridine induction in rats. This difference was coincident with a reduced number of purkinje cells at the same place (Mohammadi et al., 2017). A previous study has shown that the neuronal and neuroglial arrangement changed in the anterior cingulate cortex of patients with schizophrenia (Benes and Bird, 1987). In another study, a 3D model of the neuronal locations of the cerebral cortex was created by density maps (Cruz et al., 2008). Jinno et al. (2007) investigated the stereological spatial distribution of microglia and astrocytes in the hippocampus of mice.

The spatial distribution of the spinal neuroglial cells is related to their functions. These cells provide support and nutrition for neurons. After sciatic nerve injury, neuroglial

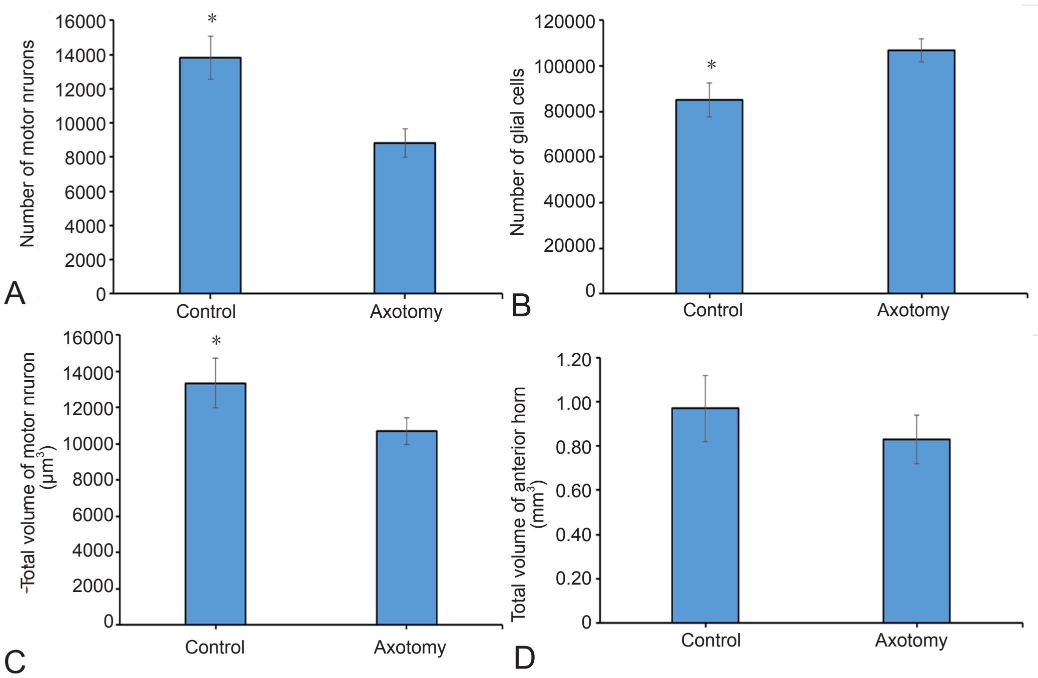

Figure 5 Representation of the estimated parameters of the anterior horn of rat spinal cord.
(A) Motoneuron number; (B) neuroglial cell number; (C) total volume of motoneurons; (D) total volume of the anterior horn in the spinal cord in the axotomy and control groups. **P* < 0.05, *vs*. axotomy group (Mann-Whitney *U* test). All data are expressed as the mean ± SD of the studied groups.

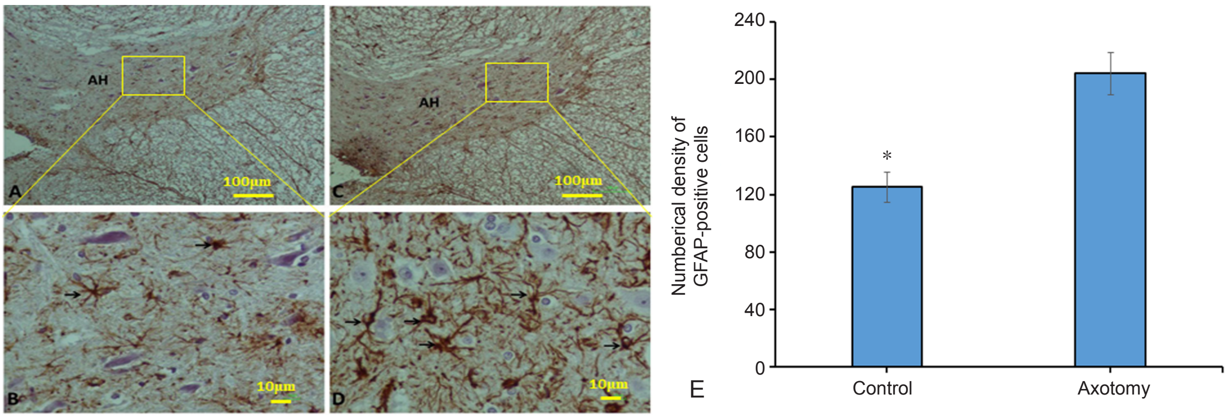

Figure 6 Astrocytic immunostaining for glial fibrillary acidic protein (GFAP) in the anterior horn of the spinal cord.
(A, B) Control group; (C, D) axotomy group (AH denotes the anterior horn, arrow denotes astrocyte). Scale bars: 100 μm in A and C, 10 μm in B and D. (E) numerical density of GFAP-positive cells in the anterior horn. **P* < 0.05, *vs*. axotomy group (Mann-Whitney *U* test). Data are expressed as the mean ± SD. GFAP: Glial fibrillary acidic protein.

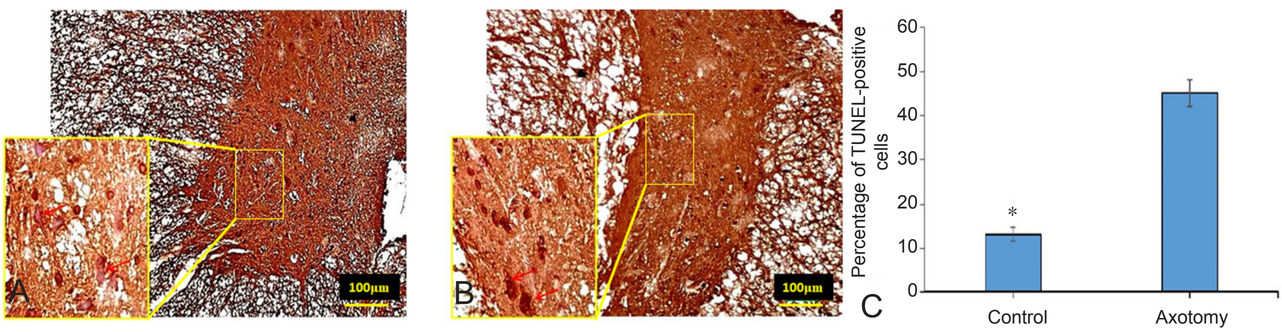

Figure 7 TUNEL detection of apoptotic anterior horn motoneurons in the axotomy and control groups.
(A) Control group; (B) axotomy group. Apoptotic cells (brown; indicated by arrows). Scale bars: 100 μm. (C) Percentage of TUNEL-positive cells in the anterior horn. **P* < 0.05, *vs*. axotomy group (Mann-Whitney *U* test). Data are expressed as the mean ± SD.

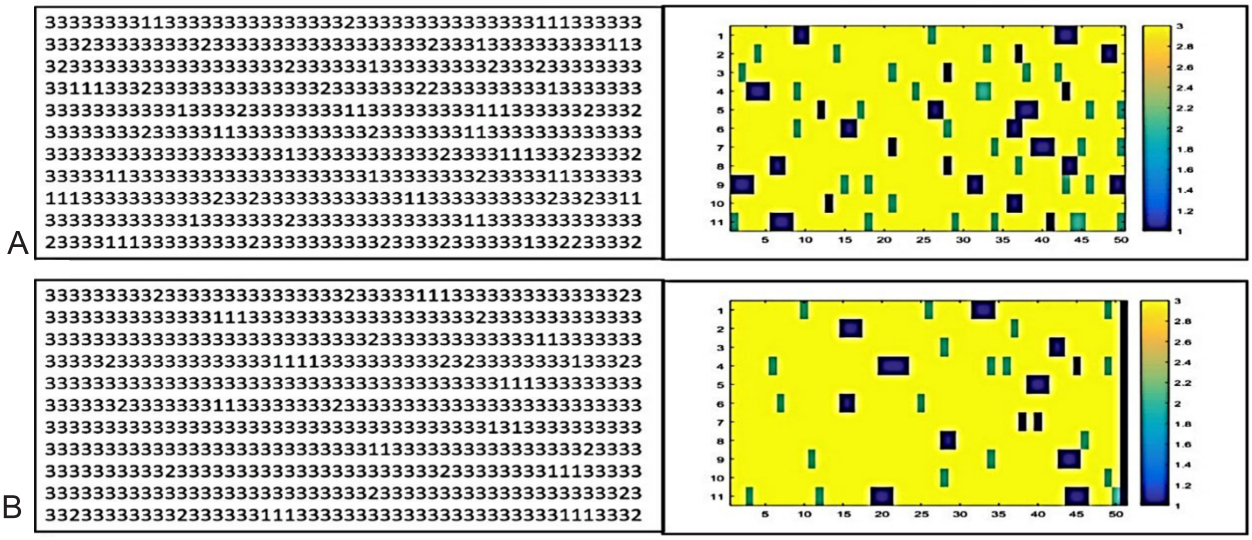

Figure 8 Conversion of data matrix to image type and display of motoneurons following sciatic nerve injury.
(1) Blue indicates motoneurons; (2) green represents neuroglial cells; (3) yellow is neuropil; (A) control group; (B) axotomy group.

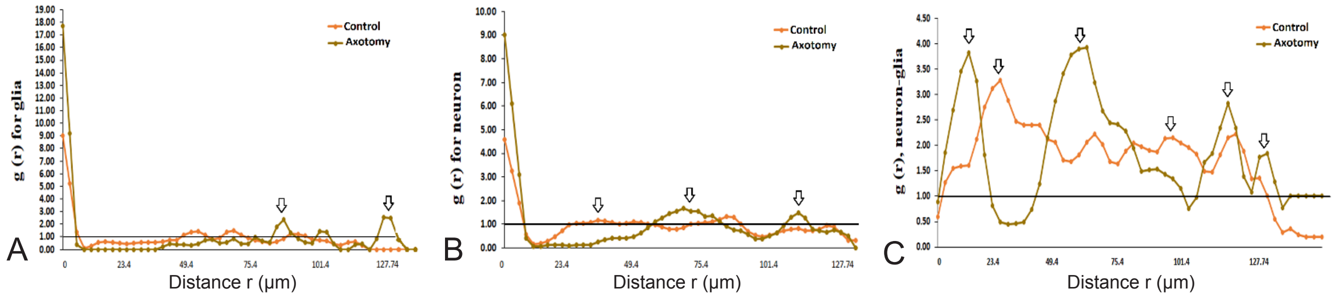

Figure 9 Spatial arrangement of neurons and glial cells in the anterior horn of the spinal cord.
(A, B) Relationship between pair correlation and dipole distance for neuroglial cells (A) and motoneurons (B) in the control and axotomy groups. Arrows denote significant differences for both groups. (C) Cross-correlation function g(r) between motoneurons and the neuroglial cells plotted against distance r (μm). The arrows show the value of the distance for which there was a significant difference in cross-correlation function between control and axotomy groups ($P < 0.05$).

cells begin to experience irreversible morphological and functional changes. The physiological and structural changes are accompanied by cell distribution alterations; however, the spatial distribution of motoneurons and neuroglial cells within a given region of the anterior horn may have important implications for the function of that region. Analysis of the spatial arrangement provides useful information about larger and smaller structures of the cells such as the renal glomeruli and cellular organelles (Mayhew, 1999a, b). In summary, our findings have provided valuable and important additional information about the spatial distribution of the anterior horn cells following sciatic nerve injury, but have not allowed us to completely understand the pathology of these cells after injury.

Conclusion

The results of this work revealed a difference between the control and axotomy groups regarding the spatial patterns of cells in the anterior horn after sciatic nerve injury. Cell-cell dissociation (a gap) was detected between the motoneurons and neuroglial cells in the anterior horn of the spinal cord following sciatic nerve injury. Although further analysis will be required, the present findings provide a key to understanding the relationship between the motoneurons and neuroglial cells.

Acknowledgments: *This article has been extracted from the thesis written by Ali Rashiadian Rashiabadi, PhD student of anatomical sciences from School of Medicine Shahid Beheshti University of Medical Sciences.*
Author contributions: *Design of study: MAA; implementation of stereological study, provision of tissue sample, collection of clinical data: ARR; preparation of animal models: ES, FH; English language and grammar editing: FFF; statistical analysis: YS, AA; drafting of article: MHH, RMF, ARR, MAA; real-time polymerase chain reaction: AR; immunohistochemistry: ARR, MAA; approval of final article for publication: all authors.*
Conflicts of interest: *The authors declare that they have no competing interests.*
Financial support: *The work was supported by the Research Vice-chancellor of Shahid Beheshti University of Medical Sciences, Tehran, Iran (No. 1394-373; to RMF).*
Institutional review board statement: *The experimental protocol was reviewed and approved by the Animal Ethics Committee of Shahid*

Beheshti University of Medical Sciences (approval No. IR.SBMU.MSP.REC1395.375) on October 17, 2016.

Copyright license agreement: *The Copyright License Agreement has been signed by all authors before publication.*

Data sharing statement: *Datasets analyzed during the current study are available from the corresponding author on reasonable request.*

Plagiarism check: *Checked twice by iThenticate.*

Peer review: *Externally peer reviewed.*

References

Altomare L, Fare' S (2008) Cells response to topographic and chemical micropatterns. J Appl Biomater Biomech 6:132-143.

Benes FM, Bird ED (1987) An analysis of the arrangement of neurons in the cingulate cortex of schizophrenic patients. Arch Gen Psychiatry 44:608-616.

Bjugn R (1993) The use of the optical disector to estimate the number of neurons, glial and endothelial cells in the spinal cord of the mouse-with a comparative note on the rat spinal cord. Brain Res 627:25-33.

Brodal A (1981) Neurological anatomy in relation to clinical medicine. New York: Oxford University Press.

Chen MH, Ren QX, Yang WF, Chen XL, Lu C, Sun J (2013) Influences of HIF-lα on Bax/Bcl-2 and VEGF expressions in rats with spinal cord injury. Int J Clin Exp Pathol 6:2312-2322.

Cruz L, Urbanc B, Inglis A, Rosene DL, Stanley HE (2008) Generating a model of the three-dimensional spatial distribution of neurons using density maps. Neuroimage 40:1105-1115.

Ekerdt BL, Segalman RA, Schaffer DV (2013) Spatial organization of cell-adhesive ligands for advanced cell culture. Biotechnol J 8:1411-1423.

Gelderd JB, Chopin SF (1977) The vertebral level of origin of spinal nerves in the rat. Anat Rec 188:45-47.

Griffin JW, George EB, Hsieh S, Glass JD (1995) Axonal degeneration and disorders of the axonal cytoskeleton. In: The axon: structure, function and pathophysiology (Waxman SG, Kocsis JD, Stys PK, eds). New York: Oxford University Press.

Gundersen HJ, Bagger P, Bendtsen TF, Evans SM, Korbo L, Marcussen N, Møller A, Nielsen K, Nyengaard JR, Pakkenberg B (1988a) The new stereological tools: dissector, fractionator, nucleator and point sampled intercepts and their use in pathological research and diagnosis. APMIS 96:857-881.

Gundersen HJ, Bendtsen TF, Korbo L, Marcussen N, Møller A, Nielsen K, Nyengaard JR, Pakkenberg B, Sørensen FB, Vesterby A (1988b) Some new, simple and efficient stereological methods and their use in pathological research and diagnosis. APMIS 96:379-394.

Gundersen HJ, Jensen EB (1987) The efficiency of systematic sampling in stereology and its prediction. J Microsc 147:229-263.

Jinno S, Fleischer F, Eckel S, Schmidt V, Kosaka T (2007) Spatial arrangement of microglia in the mouse hippocampus: a stereological study in comparison with astrocytes. Glia 55:1334-1347.

Kakinohana O, Cizkova D, Tomori Z, Hedlund E, Marsala S, Isacson O, Marsala M (2004) Region-specific cell grafting into cervical and lumbar spinal cord in rat: a qualitative and quantitative stereological study. Exp Neurol 190:122-132.

Krasnoperov RA, Stoyan D (2004) Second-order stereology of spatial fiber systems. J Microsc 216:156-164.

Li Q, Liu Y, Li M, Wu YM, Zeng L, Li YY (2006) The difference of nerve growth factor and ciliary neurotrophic factor between the sensitive and motor fibres regeneration. Zhonghua Zheng Xing Wai Ke Za Zhi 22:371-374.

Low HL, Nogradi A, Vrbová G, Greensmith L (2003) Axotomized motoneurons can be rescued from cell death by peripheral nerve grafts: the effect of donor age. J Neuropathol Exp Neurol 62:75-87.

Lu XM, Shu YH, Qiu CH, Chen KT, Wang YT (2014) Protective effects and anti-apoptotic role of nerve growth factor on spinal cord neurons in sciatic nerve-injured rats. Neurol Res 36:814-823.

Manetto V, Sternberger NH, Perry G, Sternberger LA, Gambetti P (1988) Phosphorylation of neurofilaments is altered in amyotrophic lateral sclerosis. J Neuropathol Exp Neurol 47:642-653.

Martin LJ (1999) Neuronal death in amyotrophic lateral sclerosis is apoptosis: possible contribution of a programmed cell death mechanism. J Neuropathol Exp Neurol 58:459-471.

Mattfeldt T, Eckel S, Fleischer F, Schmidt V (2006) Statistical analysis of reduced pair correlation functions of capillaries in the prostate gland. J Microsc 223:107-119.

Mattfeldt T, Frey H, Rose C (1993) Second-order stereology of benign and malignant alterations of the human mammary gland. J Microsc 171:143-151.

Mayhew TM (1979) Basic stereological relationships for quantitative microscopical anatomy--a simple systematic approach. J Anat 129(Pt 1):95-105.

Mayhew TM (1999a) Quantitative description of the spatial arrangement of organelles in a polarised secretory epithelial cell: the salivary gland acinar cell. J Anat 194:279-285.

Mayhew TM (1999b) Second-order stereology and ultrastructural examination ofthe spatial arrangements of tissue compartments within glomeruli of normal and diabetic kidneys. J Microsc 195:87-95.

Mohammadi R, Heidari MH, Sadeghi Y, Abdollahifar MA, Aghaei A (2017) Evaluation of the spatial arrangement of Purkinje cells in ataxic rat's cerebellum after Sertoli cells transplantation. Folia Morphol (Warsz) 77:194-200.

Munoz DG, Greene C, Perl DP, Selkoe DJ (1988) Accumulation of phosphorylated neurofilaments in anterior horn motor neurons of amyotrophic lateral sclerosis patients. J Neuropathol Exp Neurol 47:9-18.

Nakamura SI, Myers RR (2000) Injury to dorsal root ganglia alters innervation of spinal cord dorsal horn lamina involved in nociception. Spine (Phila Pa 1976) 25:537-542.

Noorafshan A, Abdollahifar MA, Asadi-Golshan R, Rashidian-Rashidabadi A, Karbalay-Doust S (2014) Curcumin and sertraline prevent the reduction of the number of neurons and glial cells and the volume of rats' medial prefrontal cortex induced by stress. Acta Neurobiol Exp (Wars) 74:44-53.

Noorafshan A, Abdollahifar MA, Karbalay-Doust S (2015) Stress changes the spatial arrangement of neurons and glial cells of medial prefrontal cortex and sertraline and curcumin prevent it. Psychiatry Investig 12:73-80.

Oppenheim RW, Houenou LJ, Johnson JE, Lin LF, Li L, Lo AC, Newsome AL, Prevette DM, Wang S (1995) Developing motor neurons rescued from programmed and axotomy-induced cell death by GDNF. Nature 373:344-346.

Preyat N, Rossi M, Kers J, Chen L, Bertin J, Gough PJ, Le Moine A, Rongvaux A, Van Gool F, Leo O (2015) Intracellular nicotinamide adenine dinucleotide promotes TNF-induced necroptosis in a sirtuin-dependent manner. Cell Death Differ 23:29-40.

Reed MG, Howard CV (1999) Stereological estimation of covariance using lineardipole probes. J Microsc 195:96-103.

Reed MG, Howard CV, DE Yanés GS (2010) One-stop stereology: the estimation of 3D parameters using isotropic rulers. J Microsc 239:54-65.

Sendtner M, Holtmann B, Kolbeck R, Thoenen H, Barde YA (1992) Brain derived neurotrophic factor prevents the death of motoneurons in newborn rats after nerve transection. Nature 360:757-759.

Sun W, Sun C, Lin H, Zhao H, Wang J, Ma H, Chen B, Xiao Z, Dai J (2009a) The effect of collagen-binding NGF-beta on the promotion of sciatic nerve regeneration in a rat sciatic nerve crush injury model. Biomaterials 30:4649-4656.

Sun W, Sun C, Zhao H, Lin H, Han Q, Wang J, Ma H, Chen B, Xiao Z, Dai J (2009b) Improvement of sciatic nerve regeneration using laminin-binding human NGF-beta. PLoS One 4: e6180.

Tong JX, Rich KM (1997) Diphenylpiperazines enhance regeneration after facial nerve injury. J Neurocytol 26:339-347.

Walloe S, Nissen UV, Berg RW, Hounsgaard J, Pakkenberg B (2011) Stereological estimate of the total number of neurons in spinal segment D9 of the red-eared turtle. J Neurosci 31:2431-2435.

Yin ZS, Zhang H, Bo W, Gao W (2010) Erythropoietin promotes functional recovery and enhances nerve regeneration after peripheral nerve injury in rats. AJNR Am J Neuroradiol 31:509-515.

C-Editor: Zhao M; S-Editor: Li CH; L-Editor: Song LP; T-Editor: Jia Y